Signatures of Open and Noisy Quantum Systems in Single-Qubit Quantum Annealing

Zachary Morrell,[1,*] Marc Vuffray,[1] Andrey Y. Lokhov,[1] Andreas Bärtschi,[1] Tameem Albash,[2,3,4] and Carleton Coffrin[1]

[1] *Los Alamos National Laboratory, Los Alamos, New Mexico 87545, USA*

[2] *Department of Electrical & Computer Engineering, University of New Mexico, Albuquerque, New Mexico 87131, USA*

[3] *Department of Physics & Astronomy, University of New Mexico, Albuquerque, New Mexico 87131, USA*

[4] *Center for Quantum Information and Control (CQuIC), University of New Mexico, Albuquerque, New Mexico 87131, USA*

(Received 30 August 2022; revised 1 December 2022; accepted 25 January 2023; published 16 March 2023)

We propose a quantum annealing protocol that effectively probes the dynamics of a single qubit on D-Wave's quantum annealing hardware. This protocol uses D-Wave's *h*-gain schedule functionality, which allows the rapid suppression of the longitudinal magnetic field at arbitrary points during the anneal. This feature enables us to distinguish between open and closed-system dynamics as well as the presence and absence of longitudinal magnetic field noise. We show that thermal fluctuations alone are not sufficient to explain the system's dynamics and that a prominent role is played by magnetic field fluctuations, which need to be included in an open quantum system description. Moreover, our protocol only requires single-qubit measurements, which makes it suitable as an exploration and calibration tool for large-scale quantum annealing hardware.

DOI: 10.1103/PhysRevApplied.19.034053

I. INTRODUCTION

Quantum annealing is an analog computing approach for preparing low-energy eigenstates of classical and quantum Hamiltonians [1–4]. At the heart of the algorithm is the adiabatic theorem [5–7], which guarantees that a quantum system initially prepared in the ground state of a time-evolving Hamiltonian will remain with high probability in the instantaneous ground state at later times as long as the evolution satisfies an adiabatic condition. Quantum annealing exploits this property by slowly interpolating between a Hamiltonian for which the ground state is known and a target Hamiltonian that we wish to minimize [1,3,4]. An advantage of quantum annealing over gate-based implementations of quantum computation is its minimal control requirements [8–11]: generically, the qubits are annealed uniformly and slowly, which in principle makes it readily scalable to thousands of qubits. For this reason, quantum annealing remains a promising quantum optimization metaheuristic in the noisy intermediate-scale quantum era [12], with the hope that it may provide some advantage over classical algorithms. However, just like any other analog computing method, quantum annealing is sensitive to hardware defects, limited controller accuracy [13,14], and other sorts of spurious effects and noise that are inherently present in any physical system.

Today's largest and most mature quantum annealers are produced by D-Wave Systems with a qubit technology based on superconducting loops [15–19]. There is still an ongoing research effort to probe the effectiveness of the D-Wave hardware as an optimization tool [20–23], as well as a Gibbs sampler [24–33], which could prove useful in machine learning applications. With the latest systems from D-Wave, featuring thousands of qubits, it remains important to identify the noise sources and their effects on the output statistics in order to discover further use cases for the hardware.

In this paper, we test four different categories of dynamic models against D-Wave measurements and see if they have the power to reproduce the machine's behavior. These four categories aim to answer two different fundamental questions: how the annealing dynamics is affected by its environment (closed versus open systems), and how consistent the programmed Hamiltonian is over consecutive annealing runs (single versus mixture of random Hamiltonians). These models are effectively trying to reproduce the effect of noise over two different time scales,

*zmorrell@lanl.gov

fast and slow, with respect to the typical annealing time. Thermal fluctuations correspond to fast time scales since they account for changes in the state on the time scale of a single annealing run, while changes over multiple annealing runs, being on larger time scales compared to a single anneal, are modeled by a mixture of Hamiltonians with random longitudinal fields.

A lot of effort has been devoted to finding signatures of thermal fluctuations in the D-Wave output statistics, which are typically modeled within an open system paradigm. The advent of quantum annealing hardware has reignited development of open system descriptions for systems with time-dependent Hamiltonians (for recent advancements, see [34–36]). To model the effect of thermal fluctuations, we use the adiabatic master equation (AME) [37,38] to describe the output statistics of the D-Wave hardware. The AME gives a description of dissipative dynamics under the assumption of a weak coupling to a finite temperature environment as well as slow evolution relative to the dynamical time scales of the environment. This description has been successful at giving qualitative agreement for slow annealing processes on D-Wave processors [39–41]. The AME's success stems from the fact that the instantaneous steady state of the dynamics is the Gibbs state associated with the instantaneous Hamiltonian, hence it captures qualitatively the loss of population from the ground state due to thermal excitation when the ground state energy gap becomes smaller than the temperature, with the rate of population loss controlled by the system-bath coupling that can be tuned to give the best possible fit to experimental data. However, the AME's applicability is limited and is expected to break down near small energy gaps where the weak-coupling assumption is violated. Simulations using the polaron transformation [42] (also called the noninteracting blip approximation [43]) that allow investigations beyond the weak-coupling limit give the strongest quantitative agreement with the D-Wave hardware [44], but this approach tends to be limited to the lowest-lying energy levels of the system. The simplicity and interpretability of the AME make it a convenient choice.

To model fluctuations in the programmed Hamiltonian, we use randomness in its parameters. Mixtures of random Hamiltonians with longitudinal field noise have been shown to play a major role in explaining the formation of the anomalous single-qubit response to magnetic field changes [31,32] and of the effective spurious links [31,33].

One of the primary criticisms of the D-Wave hardware is that its output statistics can often be captured by simple classical models, such as the spin-vector Monte Carlo (SVMC) algorithm [45,46] or spin-vector Langevin dynamics [39,47]. These methods provide descriptions of evolutions in the semiclassical energy landscape of the qubit system [48], which turns out to coincide well with the dynamics of superconducting flux qubits in the strong system-bath coupling limit [49]. While these descriptions can quite often describe many qualitative features of the hardware, they do not necessarily reproduce all experimental results [40]. Our aim in this work is not to make a claim that the output statistics can *only* be described by a fully quantum open system description. Instead, we will show that a quantum description of the dynamics requires both thermal and magnetic field fluctuations to fully account for the system's behavior.

One main challenge in modeling the D-Wave hardware dynamics is that many experimental parameters are fixed and cannot be tuned by the user: the state preparation is predetermined and the system can only be measured at the end of the anneal in the computational basis. Therefore, there exists a substantial risk of overfitting observations with different types of models when we consider large systems with multiple spins and complex interactions. A key ingredient that we introduce to overcome data scarcity is what we call the h-stop protocol that currently can be performed only for systems without couplings. This modification of the annealing protocol effectively enables us to get information about the state of the system during the dynamics. Leveraging this protocol, we will demonstrate that both *thermal fluctuations* and *longitudinal field noise* are necessary ingredients to explain the dynamic properties measured in the D-Wave hardware. In particular, we show that the h-stop protocol dynamics cannot be reproduced with thermal fluctuations alone, even though it can be approximated with closed-system dynamics and longitudinal field noise at small annealing time and input magnetic field. This highlights the importance of slower fluctuations in the D-Wave quantum annealing dynamics.

II. BACKGROUND AND DYNAMIC MODELS

The Hamiltonian realized in the D-Wave quantum annealers is the transverse field Ising model

$$H(s) = -A(s)\sum_i \xi_i \sigma_i^x + B(s)\left(\sum_i h_i \sigma_i^z + \sum_{i<j} J_{ij}\sigma_i^z\sigma_j^z\right) \tag{1}$$

where the annealing schedule is defined by functions $A(s)$ and $B(s)$, with normalized time parameter $s = t/\tau$, where $t \in [0, \tau]$ is the current time in the anneal and τ is the total anneal time. The programmed transverse field strength and the programmed longitudinal field strength on qubit i are given by ξ_i and h_i, respectively. The coupling strength between qubits i and j is given by J_{ij}. The user is only able to modify the programmed longitudinal field strengths and coupling strengths. The Pauli operators on each qubit are given by σ_i^x and σ_i^z, and measurements are performed in the computational basis, such that $|0\rangle = |\uparrow\rangle$ and $|1\rangle = |\downarrow\rangle$. The state of the system is described by its density matrix $\rho(s)$ which is initially prepared in the

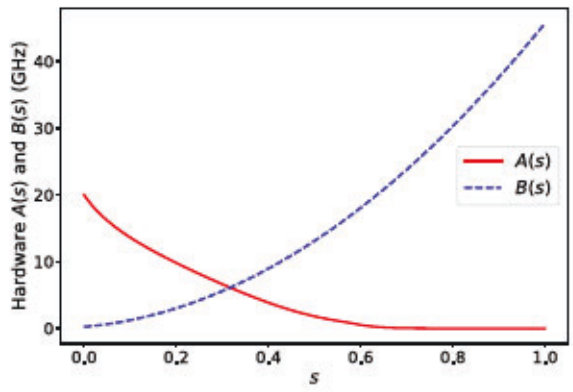

FIG. 1. The D-Wave default annealing schedule for the DW_2000Q_LANL system. The red line and the blue dashed line represent the annealing schedules $A(s)$ and $B(s)$ in Eq. (1), respectively. The unit of energy of the annealing schedule is expressed in hertz after setting $\hbar = 1$.

ground state of the Hamiltonian at $s = 0$, that is, $\rho(0) = |+\rangle\langle+|$, where $|+\rangle = \bigotimes_i (1/\sqrt{2})(|\uparrow\rangle + |\downarrow\rangle)$. The annealing protocol slowly interpolates between a transverse field Hamiltonian and the target Ising Hamiltonian on the longitudinal component, that is, $A(0) \gg B(0)$ and $A(1) \ll B(1)$ (see Fig. 1). It is customary to measure energy in units of $\hbar$ (or equivalently set $\hbar = 1$), with the convention that fields and couplings are dimensionless and the annealing is expressed in hertz.

For our experiments, we made use of the DW 2000Q hardware from D-Wave Systems, which was maintained by Los Alamos National Laboratory. On the 2000Q chip, D-Wave uses superconducting flux qubits to implement a quantum annealer with a so-called Chimera graph connection topology [19,50]. In the present work, we focus our attention on single qubits; the topology plays no role in our study as we set all coupling strengths to $J_{ij} = 0$.

In what follows, we go through the different dynamic models that we consider to encode the time evolution of the density matrix.

A. Closed quantum systems

A closed quantum system simulation assumes that the interactions between the environment and the system are negligible. Therefore, the evolution of the density matrix is described by the von Neumann equation

$$\frac{d}{ds}\rho(s) = -i\tau[H(s), \rho(s)], \tag{2}$$

where we have set $\hbar = 1$. We solve the von Neumann equation numerically using a fourth-order integration method based on the Magnus expansion [51]. Equation (2) is the simplest way to represent the evolution of a quantum system. However, interactions with the environment are often unavoidable, so it is critical to understand what behavior can be induced by such interactions. This leads to the challenge of simulating an open quantum system.

B. Open quantum systems

We choose to model the open system dynamics using the AME [38], which is a master equation in Lindblad form [52] given by

$$\frac{1}{\tau}\frac{d}{ds}\rho(s) = -i[H(s), \rho(s)] + \sum_i \sum_\omega \gamma(\omega)\left[L_{\omega i}(s)\rho(s)L_{\omega i}^\dagger(s) - \frac{1}{2}\left\{L_{\omega i}^\dagger(s)L_{\omega i}(s), \rho(s)\right\}\right] \tag{3}$$

where $\gamma(\omega)$ encodes properties of the bath and satisfies the Kubo-Martin-Schwinger condition $\gamma(-\omega) = e^{-\beta\omega}\gamma(\omega)$ [53–55]. The sum over ω is the sum over all Bohr frequencies (differences of all possible energy eigenvalues of $H(s)$), and the sum over i is over all system-bath interaction terms. We assume that each qubit interacts with an independent yet identical Ohmic heat bath of harmonic oscillators, such that

$$\gamma(\omega) = 2\pi g^2 \frac{\omega e^{-|\omega|/\omega_c}}{1 - e^{-\beta\omega}} \tag{4}$$

where ω_c is the cutoff frequency and the Lindblad operators are then given by

$$L_{\omega i} = \sum_{a,b} \delta_{\omega, E_b(s) - E_a(s)} \langle E_a(s)|\sigma_i^z|E_b(s)\rangle |E_a(s)\rangle\langle E_b(s)| \tag{5}$$

where we have assumed a σ^z system-bath interaction for each qubit and $|E_a(s)\rangle$ are the instantaneous eigenstates of the Hamiltonian with eigenvalues $E_a(s)$.

C. Longitudinal field noise

The density matrix $\rho(s)$ can only be observed indirectly through projective measurements. In order to obtain good-quality estimates of the outcome probabilities, it is necessary to repeat the same experiment numerous times. However, interactions in the system can slowly change between runs due to limitations on the controller accuracy or slowly evolving exogenous sources of noise. We model this process using a mixture of random Hamiltonians, where fluctuations take place on the longitudinal field. More precisely, the random Hamiltonian describing a single qubit is modeled via the expression

$$H(s) = -A(s)\xi\sigma^x + B(s)h\sigma^z + B(1)\Delta z\sigma^z, \tag{6}$$

where $\Delta z \sim \mathcal{N}(\mu_{\Delta z}, \sigma_{\Delta z})$ represents a longitudinal field that is constant and independent of time during a single

anneal but takes a random value for different anneals. The random contribution is rescaled by $B(1)$, allowing for the mean and standard deviations of the distribution to be interpreted by their scale relative to the maximum programmed longitudinal field. The simulation of the mixture of random Hamiltonians is realized by running either the von Neumann equation (2) or the AME (3) 1000 times with Δz being resampled for each simulation. The final density matrix of the mixture is the average of the density matrices that we obtained for different values of Δz.

III. EXPERIMENTS AND RESULTS

We test the predictive power of our models that describe a closed or an open quantum system with and without longitudinal field noise. For simplicity, we will refer to these models as closed-open and noisy-noiseless models. Our experiments involve collecting the output probability distribution of a single-qubit system for different values of the input parameters and then comparing the data to the predictions of our different models where the parameters of the models are fitted to best reproduce the experimental results. More details on the fitting procedure can be found in Appendix A. We consider two different data collection and annealing protocols: the h-sweep protocol and the h-stop protocol. All of the data were obtained from the now decommissioned DW_2000Q_LANL system.

A. h-sweep protocol

The default annealing protocol of D-Wave's application programming interface uses the annealing schedule functions shown in Fig. 1. We question what sort of noise signatures can be observed with this default annealing schedule and whether these signatures can be used to differentiate between an open and a closed quantum system's evolution. For a single spin, the two parameters that can be modified are the annealing time τ and the longitudinal field h. For different annealing time, we sweep over several h values to see how the output probabilities change, as was done in [32]. We refer to this type of experiment as the h-sweep protocol. For our h-sweep experiments, we took 1 million samples for each h value, sweeping over $h = \{0.025, 0.050, \ldots, 1.0\}$.

The results of the h-sweep protocol and the best fit for closed systems with and without random longitudinal field noise are shown in Fig. 2. The hardware exhibits a drop in the probability of measuring $|\downarrow\rangle$ at small h, which the closed-noiseless simulations do not exhibit. For the closed-noiseless simulations, the evolution is adiabatic even for the lowest h and τ values used, so the probability is effectively 1. However, the closed-noisy and open-noiseless simulations reproduce the drop in probability of the hardware for distinctly different reasons. In the open-noiseless case, thermal excitations out of the ground state are less suppressed at small h, leading to a loss of population to the $|\uparrow\rangle$ state. For the closed-noisy case, the noise can more readily change the direction of the longitudinal field at small h, leading to a large fraction of the runs resulting in the $|\uparrow\rangle$ state. This experiment demonstrates that the single-qubit dynamics cannot be reproduced by a simple closed-system model, particularly for small values of the magnetic field. However, a closed-noisy model cannot be distinguished from an open-noiseless model with this type of experiment. Thermal fluctuations or random mixture of longitudinal fields induce a similar type of behavior in response to a change in the input magnetic field.

B. h-stop protocol

The h-sweep protocol demonstrates the limitations of the default annealing schedule in discriminating between different dynamical models, and it is necessary to implement a richer class of protocols. One possible approach is to use D-Wave's annealing-schedule controls to hold $A(s)$ and $B(s)$ constant for a certain period of time to allow for thermalization effects to take place, as is done by Ref. [41]. Unfortunately, a protocol like this generally requires the use of more qubits in order to glean useful information, which can lead to model overfitting and becomes challenging to simulate efficiently when performing thousands of noise realizations.

Another approach is to use an annealing schedule with a quench at various s values throughout the anneal to approximate instantaneous measurements, as described in Ref. [56]. This procedure hopes that the system will not have the time to respond to the rapid changes in the annealing rate. Unfortunately, the current quench rates on the hardware are not short enough for single-qubit quenches, since the system still tends to reach the final ground state with high probability.

We will show that it is possible to obtain interesting measurement statistics by making use of D-Wave's h-gain schedule functionality [57].

D-Wave's h-gain schedule control works by introducing a user-defined function, $k(s)$ on the h parameter in the Hamiltonian. In the case of the single-qubit model with longitudinal field noise, the Hamiltonian from Eq. (1) is modified to

$$H(s) = -A(s)\xi\sigma^x + B(s)k(s)h\sigma^z + B(1)\Delta z\sigma^z. \quad (7)$$

The idea behind this modified scheduled is to obtain instantaneous snapshots of the hardware state by manipulating the $k(s)$ function, in particular by setting $k(s)$ to zero at a certain moment during the anneal. Note, however, that this procedure does not fully suspend the dynamics since the transverse field remains untouched, so our measurements are not equivalent to an instantaneous measurement.

The protocol we propose is rather simple: anneal with the standard annealing schedule (no pauses or quenches),

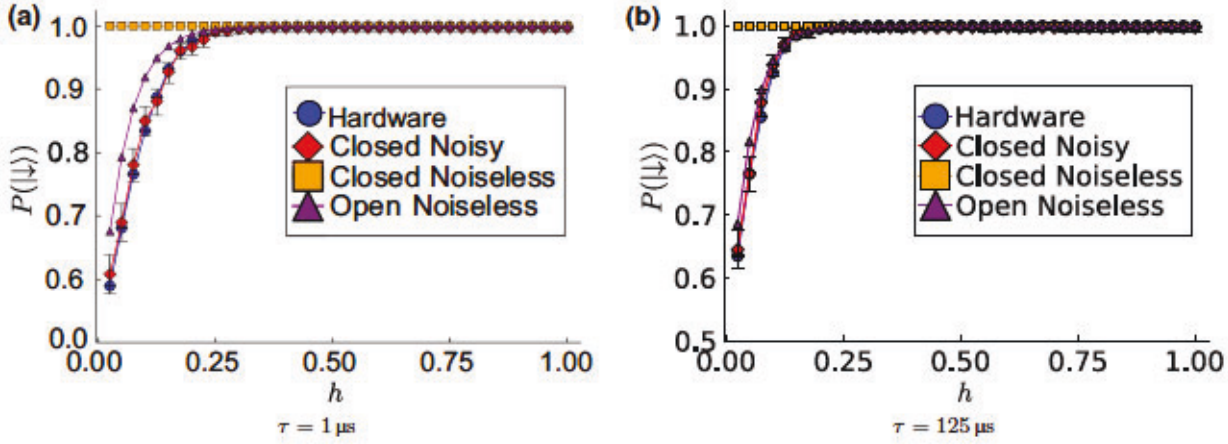

FIG. 2. Measurement probabilities $P(|\downarrow\rangle)$ at the end of the anneal with respect to input magnetic field h. The blue line represents the data sampled from the LANL_DW2000Q hardware with 1 million shots, the red line represents the simulation of the closed-noisy system, the green line represents the results of the closed-noiseless system (i.e., $\Delta z = 0$ with the hardware annealing schedules), and the purple line shows the simulation of the open-noiseless system. This figure does not include any open-noisy system simulations because the closed-noisy systems simulations already fit the data, implying open-noisy system fits would be degenerate. For the closed-noisy simulations, the standard deviation of the longitudinal field noise was found to be $\sigma_{\Delta z} = 0.05$ for $\tau = 1$ μs and $\sigma_{\Delta z} = 0.04$ for $\tau = 125$ μs. The open-noiseless simulation values shown have bath coupling strength $g^2 = 1.0 \times 10^{-4}$ for both anneal times.

and use the h-gain schedule parameter to eliminate the longitudinal field at various s values throughout the anneal. We will call this the h-stop protocol, since the user "stops" the h parameter at various points in the anneal. This protocol is a very effective way to suppress the main driving term of the dynamics because the $k(s)$ value can be reduced to 0 as quickly as 2 ns after it is at full strength, far faster than the 0.5 μs needed to perform a quench [56]. In our experiments, we chose to use an 8-ns stop time to avoid potential issues from operating at the edges of the hardware's capability. An example of this annealing schedule can be seen in Fig. 3.

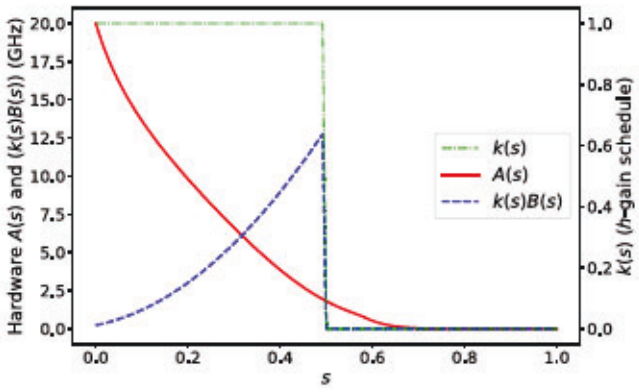

FIG. 3. Annealing schedule with the h-stop protocol. In this case, the h-gain stop finishes at $s_{\text{stop}} = 0.5$. It should be emphasized that the annealing schedule effects shown here only apply to systems where there are no coupling terms J_{ij}, since there is no coupling-gain schedule control on the D-Wave hardware at the time of writing.

In our experiments, we collected data for h-stops at points $s_{\text{stop}} \in \{0.02, 0.04, \ldots, 0.98\}$, with 1 million data points per s_{stop} and an h-stop time of 8 ns. We sampled in this manner for all input combinations of $h = \{0.025, 0.05, 0.125, 0.25, 0.5\}$ and anneal times $\tau = \{1, 5, 10, 25, 50, 125\}$ μs. We consider more points at low time values because this regime is empirically where the largest changes in the observed measurement statistics seem to occur. This is likely due to the programmed system reaching a steady state with the environmental interactions in the adiabatic limit.

Hardware results for the h-stop protocol and the model fits for the open-noiseless, closed-noisy, and open-noisy models are shown in Fig. 4 for some values of τ and h. It is important to note that the model parameters are fitted independently in each of the three different scenarios. While sweeping over s_{stop} values, we distinguish three main stages in the behavior of the system: the initial plateau, the transient, and the saturation. The initial plateau is located at around $P(|\downarrow\rangle) = 0.5$. This plateau at small s_{stop} values can be expected. The system is prepared approximately in the state $(1/\sqrt{2})(|\uparrow\rangle + |\downarrow\rangle)$, and for $s < s_{\text{stop}}$ the Hamiltonian component along x dominates that along z so that the dynamics does not change the state appreciably. When the local field is stopped, the dynamics ia still not significantly changed since the transverse field was so much larger. The transient phase takes the form of a sigmoid function and has two important features: the s_{stop} where the transition begins, and the slope of the transition. Finally, the saturation phase displays a relatively constant behavior with a saturation point that tends to $P(|\downarrow\rangle) = 1$ as τ or h increases. As we will see from our model fitting,

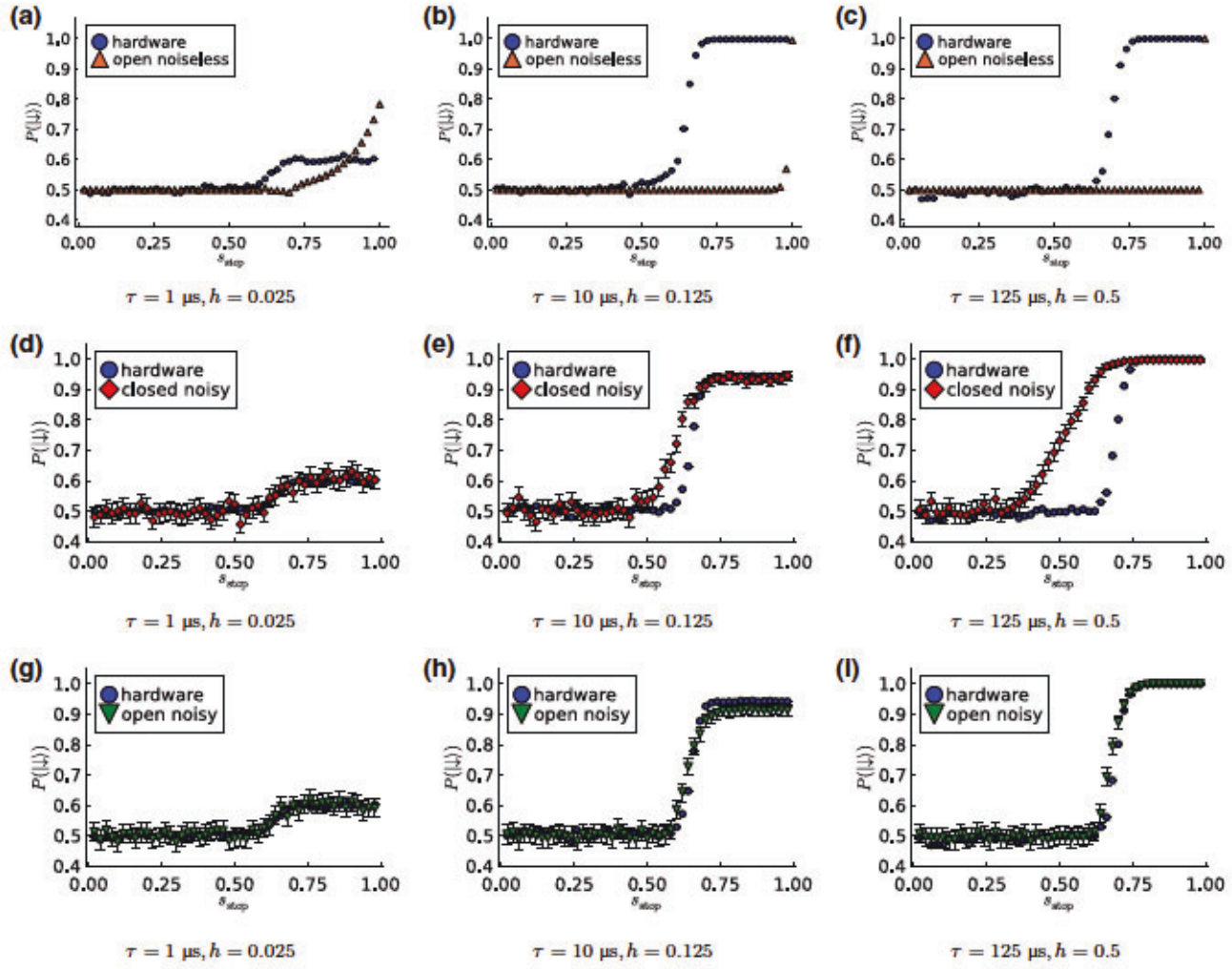

FIG. 4. Measurement probabilities $P(|\downarrow\rangle)$ with respect to s_{stop}. Each column represents different values of the annealing time τ and input magnetic field h. From left to right, column (τ, h) is (1 μs, 0.025), (10 μs, 0.125), and (125 μs, 0.5). Hardware data are shown in blue and are repeated over rows. Each row is associated with one particular model whose best fit is shown in red. From top to bottom we have the open-noiseless model, the closed-noisy model, and the open-noisy model. The three phases of the anneal can be clearly seen in Fig. 4(i). The first phase takes place approximately in the range $s_{\text{stop}} \in [0, 0.6]$, the transient in the range $s_{\text{stop}} \in [0.6, 0.8]$, and the final saturation in the range $s_{\text{stop}} \in [0.8, 1.0]$. For the open-noiseless plots (both noiseless and noisy), the coupling strength was found to be $g^2 = 1 \times 10^{-6}$. For the noisy plots, the standard deviation of the longitudinal field noise σ_{Δ_z} varied with anneal time and took the values shown in Fig. 6.

these features are a consequence of the fluctuating local field.

The worst agreement with the hardware comes from the open-noiseless model in Fig. 4. It is able to saturate at the correct observed value when $s_{\text{stop}} = 1$, which explains why it is able to reproduce the system's behavior in the h-sweep protocol in Fig. 3. However, it does so only at the very end of the anneal and therefore fails to display a transient phase in the middle of the experiment. This behavior is straightforward to understand. When the local field is stopped, the dissipative dynamics drives the system towards the thermal state of the transverse field Hamiltonian. The longer the anneal, the more time the system has to thermalize after the transverse field is turned off, but this time is reduced as s_{stop} is pushed toward 1. The absence of a saturation in this model and its presence in the other noisy model indicates how crucial a fluctuating local field is in determining the output statistics.

The closed-noisy model is able to reproduce the whole dynamics for low-input h values, and we give an example of that in Fig. 4. In this low-input regime, the fluctuating longitudinal field dominates the input local field, and since the fluctuating longitudinal field is not affected by the h-stop protocol the output can be well fitted to the model, as we have observed for the h-sweep protocol.

Furthermore, the closed-noisy model is able to reproduce the saturation at large s_{stop} values observed on the hardware. We can understand this as follows. Before

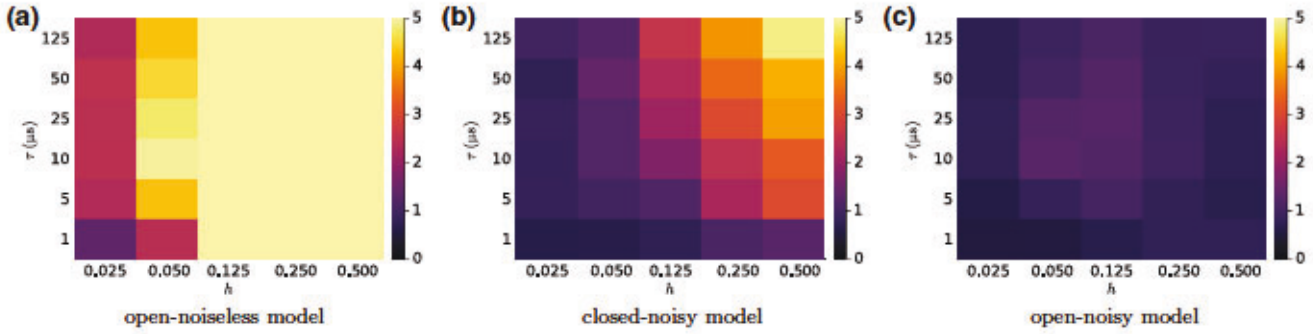

FIG. 5. These heatmaps show the ℓ_1-distance between hardware and model measurement probabilities $P(|\downarrow\rangle)$ with respect to s_{stop}. The color scale is identical across heatmaps.

the local field is stopped at a large value of s_{stop}, the Hamiltonian is composed of a weak transverse field and a strong longitudinal field, $H(s_{\text{stop}}) = -A(s_{\text{stop}})\xi\sigma^x + B(s_{\text{stop}})h\sigma^z + B(1)\Delta z\sigma^z$. If the evolution was approximately adiabatic up to this point, then the state of the system will effectively be in one of the two computational basis states, depending on the direction of the longitudinal field. The remaining part of the anneal is governed by the Hamiltonian, $H(s) = -A(s)\xi\sigma^x + B(1)\Delta z\sigma^z$, which is still dominated by the longitudinal component and will only cause the state to precess around a slowly time-varying axis that is mostly along the z direction. Thus, we can expect the noisy model to reproduce the hardware results in the regime of large s_{stop} values irrespective of the value of h.

However, we observe stark deviations compared to what is observed on the hardware for large values of h and τ, where the noisy model predicts a transition at an earlier time and with a more gradual slope compared to what is observed on the hardware. Note that the coupling with the environment is expected to play a more prominent role in this latter scenario. It is worth noting that in all cases, the saturation point is reproduced accurately in agreement with the capacity of this model to fit the h-sweep experiment in Fig. 2.

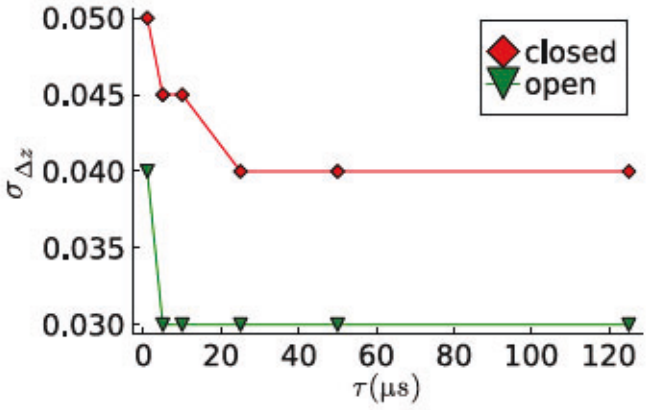

FIG. 6. Fitted standard deviation $\sigma_{\Delta z}$ for the longitudinal field noise in Eq. (6) for closed-noisy and open-noisy system models.

Finally, we observe that the open-noisy model in Fig. 4 is able to reproduce faithfully all the features that we observe from the hardware data. In particular, the transient location and slope are correctly replicated for large values of input field and large annealing time. This indicates that both the dissipative dynamics and the longitudinal field noise strongly affect the dynamics after s_{stop}. Specifically, the dissipative dynamics drives the system towards the thermal state of a Hamiltonian with a decaying x component and fixed z component.

The capacity of our models to reproduce experimental results for the entire range of annealing time and input magnetic fields is summarized in Fig. 5. The quality metric for the fit is the area between the experimental and the model measurement probabilities $P(|\downarrow\rangle)$ with respect to s_{stop}. The previous examples from Fig. 4 appear in the bottom-left corner, center, and upper-right corner of their respective heatmaps in Fig. 5. As seen earlier, the open-noiseless model turns out to reproduce poorly the system's behavior for the entire range of parameters, while the closed-noisy model tends to struggle only for the larger values of magnetic field and annealing time. In contrast, the open-noisy model performs systematically better than the other two models and its fit quality is uniform over the entire range of input parameters.

At this stage, it should not be surprising that the open-noisy model outperforms the other candidates. Indeed, the open-noisy model has more adjustable parameters than every other model and therefore its fitting capacity is the highest among them. It remains to be known if the remarkable explanatory power of the open-noisy model is due to overfitting, or whether this is an indication that the model is rooted in physical ground. We recall that the adjustable parameters are the bath coupling strength g^2, the longitudinal field noise mean $\mu_{\Delta z}$, and standard deviation $\sigma_{\Delta z}$.

With our fitting procedure, we find that a bath coupling strength and longitudinal field noise mean value were

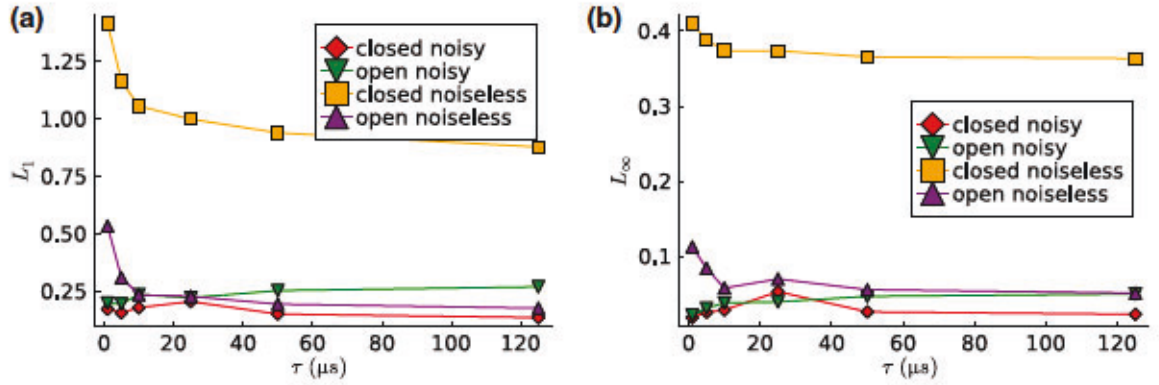

FIG. 7. These plots show the distance from the hardware for the h-sweep experiment. The parameters used to determine the models used in this experiment were also used to determine the s-sweep experiment, which is why the open system seems to show a slightly worse fit. This disparity can change depending on the distance metric and how well the h-stop experiment is fitted.

unaffected by the input anneal times and magnetic fields. Therefore, the bath coupling strength and longitudinal field noise mean value are set to $g^2 = 1.0 \times 10^{-6}$ and $\mu_{\Delta z} = 0$ for all models. The longitudinal field noise standard deviation is found to be unaffected by the input magnetic field. Nevertheless, the standard deviation is different for the closed and open models and changing with respect to the annealing time as shown in Fig. 6. For the closed system, the standard deviation tends to decrease with the annealing time, a behavior that was already noticed via h-sweep experiments in [32]. This may be caused by the inherent inability of the closed system to take into account the environment interactions that will be more prominent for longer annealing times. On the other hand, the open-noisy system has a standard deviation that remains constant for annealing times greater than 1 μs. Therefore, with the exception of annealing times $\tau = 1$ μs, the parameters of the open-noisy system are set uniformly to $g^2 = 1.0 \times 10^{-6}$, $\mu_{\Delta z} = 0$, and $\sigma_{\Delta z} = 0.028$.

Overly fluctuating parameters g^2, $\mu_{\Delta z}$, and $\sigma_{\Delta z}$ with respect to the experimental setting defined by the annealing time τ and input magnetic field h would have been interpreted as a signature of overfitting the parameters of the open-noisy model. However, we see that the model parameters remain primarily constant between experiments, as is expected, for they are believed to be mostly physically unaffected by the choice of experimental settings. The different behavior of the standard deviation at $\tau = 1$ μs for the open-noisy model is intriguing and may indicate discrepancies between the open-noisy dynamics and the actual noise dynamics. The AME makes assumptions about a separation between the system and bath time scales and does not include known error sources such as $1/f$ noise [58,59], but at larger annealing times both the experimental system and the simulations are close to a thermalized state, washing out possible discrepancies in the intermediate dynamics, which could account for the better agreement at larger annealing times. Further investigations on this question would be needed and we leave its study for future work.

IV. CONCLUSION

Our experiments have shown that by implementing annealing controls with the h-gain schedule option on D-Wave's quantum annealers, we obtain valuable information about the annealing dynamics. With this h-stop protocol, we are able to discriminate among several quantum dynamical models, highlighting that thermal fluctuations and longitudinal field noise are likely to be critical components that drive single-qubit annealing dynamics. The largest uncertainty between the models and hardware arises at the shortest annealing times, suggesting that access to smaller annealing times may allow us to better characterize and understand the noise. Finally, these single-qubit experiments can be used in the future as efficient calibration techniques for the bath coupling strength and field noise characteristics in the simulation of more complex Hamiltonians.

ACKNOWLEDGMENTS

We acknowledge support from the Laboratory Directed Research and Development program of Los Alamos National Laboratory under projects 20210114ER and 20210674ECR. This material is also based upon work supported by the National Science Foundation's Quantum Leap Big Idea under Grant No. OMA-1936388.

APPENDIX: MODEL FITTING

1. Parameters

The model parameters g^2 and $\sigma_{\Delta z}$ were fitted through grid search. While a more refined optimization approach may have yielded a more precise fit, due to the computational overhead of performing the noise realizations required for each iteration, grid search proved the most

straightforward to implement. To ensure that the grid search did not yield trends that would not make sense physically, we imposed some minor constraints on our model. First, we required that g^2 be fixed for all values of h and τ which were fitted. Second, we required that $\sigma_{\Delta z}$ be fixed across values of h, but allowed for variation between values of t. This method provided a good balance that allowed the data to be fitted quite well while avoiding overfitting. After performing the optimizations, we found that $g^2 = 1 \times 10^{-6}$ fitted the data well when combined with the $\sigma_{\Delta z}$ values shown in Fig. 6.

For our distance metric, we chose to use L_1 distance, though other metrics such as the L_2 and L_∞ distances could have been selected and the findings of this work would remain unchanged. The difference between the quality of the fit parameters when applied to the h-sweep model is shown in Fig. 7.

[1] A. Finnila, M. Gomez, C. Sebenik, C. Stenson, and J. Doll, Quantum annealing: A new method for minimizing multidimensional functions, Chem. Phys. Lett. **219**, 343 (1994).

[2] T. Kadowaki and H. Nishimori, Quantum annealing in the transverse Ising model, Phys. Rev. E **58**, 5355 (1998).

[3] P. Ray, B. K. Chakrabarti, and A. Chakrabarti, Sherrington-Kirkpatrick model in a transverse field: Absence of replica symmetry breaking due to quantum fluctuations, Phys. Rev. B **39**, 11828 (1989).

[4] G. E. Santoro, R. Martoňák, E. Tosatti, and R. Car, Theory of quantum annealing of an Ising spin glass, Science **295**, 2427 (2002).

[5] M. Born and V. Fock, Beweis des Adiabatensatzes, Z. für Phys. **51**, 165 (1928).

[6] T. Kato, On the adiabatic theorem of quantum mechanics, J. Phys. Soc. Jpn. **5**, 435 (1950).

[7] S. Jansen, M.-B. Ruskai, and R. Seiler, Bounds for the adiabatic approximation with applications to quantum computation, J. Math. Phys. **48**, 102111 (2007).

[8] A. M. Childs, E. Farhi, and J. Preskill, Robustness of adiabatic quantum computation, Phys. Rev. A **65**, 012322 (2001).

[9] M. S. Sarandy and D. A. Lidar, Adiabatic Quantum Computation in Open Systems, Phys. Rev. Lett. 95, 250503 (2005).

[10] J. Åberg, D. Kult, and E. Sjöqvist, Quantum adiabatic search with decoherence in the instantaneous energy eigenbasis, Phys. Rev. A **72**, 042317 (2005).

[11] J. Roland and N. J. Cerf, Noise resistance of adiabatic quantum computation using random matrix theory, Phys. Rev. A **71**, 032330 (2005).

[12] J. Preskill, Quantum computing in the NISQ era and beyond, Quantum **2**, 79 (2018).

[13] Z. Zhu, A. J. Ochoa, S. Schnabel, F. Hamze, and H. G. Katzgraber, Best-case performance of quantum annealers on native spin-glass benchmarks: How chaos can affect success probabilities, Phys. Rev. A **93**, 012317 (2016).

[14] T. Albash, V. Martin-Mayor, and I. Hen, Analog errors in Ising machines, Quantum Sci. Technol. **4**, 02LT03 (2019).

[15] M. W. Johnson, P. Bunyk, F. Maibaum, E. Tolkacheva, A. J. Berkley, E. M. Chapple, R. Harris, J. Johansson, T. Lanting, I. Perminov, E. Ladizinsky, T. Oh, and G. Rose, A scalable control system for a superconducting adiabatic quantum optimization processor, Supercond. Sci. Technol. **23**, 065004 (2010).

[16] A. J. Berkley, M. W. Johnson, P. Bunyk, R. Harris, J. Johansson, T. Lanting, E. Ladizinsky, E. Tolkacheva, M. H. S. Amin, and G. Rose, A scalable readout system for a superconducting adiabatic quantum optimization system, Supercond. Sci. Technol. **23**, 105014 (2010).

[17] R. Harris, *et al.*, Experimental investigation of an eight-qubit unit cell in a superconducting optimization processor, Phys. Rev. B **82**, 024511 (2010).

[18] M. W. Johnson, *et al.*, Quantum annealing with manufactured spins, Nature **473**, 194 (2011).

[19] P. I. Bunyk, E. M. Hoskinson, M. W. Johnson, E. Tolkacheva, F. Altomare, A. J. Berkley, R. Harris, J. P. Hilton, T. Lanting, A. J. Przybysz, and J. Whittaker, Architectural considerations in the design of a superconducting quantum annealing processor, IEEE Trans. Appl. Supercond. **24**, 1 (2014).

[20] S. Mandrà, Z. Zhu, W. Wang, A. Perdomo-Ortiz, and H. G. Katzgraber, Strengths and weaknesses of weak-strong cluster problems: A detailed overview of state-of-the-art classical heuristics versus quantum approaches, Phys. Rev. A **94**, 022337 (2016).

[21] S. Mandrà and H. G. Katzgraber, A deceptive step towards quantum speedup detection, Quantum Sci. Technol. **3**, 04LT01 (2018).

[22] Y. Pang, C. Coffrin, A. Y. Lokhov, and M. Vuffray, The potential of quantum annealing for rapid solution structure identification, Constraints **26**, 1 (2021).

[23] M. Kowalsky, T. Albash, I. Hen, and D. A. Lidar, 3-regular three-XORSAT planted solutions benchmark of classical and quantum heuristic optimizers, Quantum Sci. Technol. **7**, 025008 (2022).

[24] M. H. Amin, Searching for quantum speedup in quasistatic quantum annealers, Phys. Rev. A **92**, 052323 (2015).

[25] A. Perdomo-Ortiz, B. O'Gorman, J. Fluegemann, R. Biswas, and V. N. Smelyanskiy, Determination and correction of persistent biases in quantum annealers, Sci. Rep. **6**, 18628 (2016).

[26] J. Raymond, S. Yarkoni, and E. Andriyash, Global warming: Temperature estimation in annealers, Front. ICT **3**, 23 (2016).

[27] M. Benedetti, J. Realpe-Gómez, R. Biswas, and A. Perdomo-Ortiz, Estimation of effective temperatures in quantum annealers for sampling applications: A case study with possible applications in deep learning, Phys. Rev. A **94**, 022308 (2016).

[28] M. Benedetti, J. Realpe-Gómez, R. Biswas, and A. Perdomo-Ortiz, Quantum-Assisted Learning of Hardware-Embedded Probabilistic Graphical Models, Phys. Rev. X **7**, 041052 (2017).

[29] J. Marshall, E. G. Rieffel, and I. Hen, Thermalization, Freeze-out, and Noise: Deciphering Experimental Quantum Annealers, Phys. Rev. Appl. **8**, 064025 (2017).

[30] R. Li, T. Albash, and D. A. Lidar, Limitations of error corrected quantum annealing in improving the performance of Boltzmann machines, Quantum Sci. Technol. **5**, 045010 (2020).

[31] M. Vuffray, C. Coffrin, Y. A. Kharkov, and A. Y. Lokhov, Programmable Quantum Annealers as Noisy Gibbs Samplers, PRX Quantum **3**, 020317 (2022).

[32] J. Nelson, M. Vuffray, A. Y. Lokhov, and C. Coffrin, Single-qubit fidelity assessment of quantum annealing hardware, IEEE Trans. Quantum Eng. **2**, 1 (2021).

[33] J. Nelson, M. Vuffray, A. Y. Lokhov, T. Albash, and C. Coffrin, High-Quality Thermal Gibbs Sampling with Quantum Annealing Hardware, Phys. Rev. Appl. **17**, 044046 (2022).

[34] A. Y. Smirnov and M. H. Amin, Theory of open quantum dynamics with hybrid noise, New J. Phys. **20**, 103037 (2018).

[35] E. Mozgunov and D. Lidar, Completely positive master equation for arbitrary driving and small level spacing, Quantum **4**, 227 (2020).

[36] H. Chen and D. A. Lidar, Hamiltonian open quantum system toolkit, Commun. Phys. **5**, 112 (2022).

[37] E. B. Davies and H. Spohn, Open quantum systems with time-dependent Hamiltonians and their linear response, J. Stat. Phys. **19**, 511 (1978).

[38] T. Albash, S. Boixo, D. A. Lidar, and P. Zanardi, Quantum adiabatic Markovian master equations, New J. Phys. **14**, 123016 (2012).

[39] T. Albash, W. Vinci, A. Mishra, P. A. Warburton, and D. A. Lidar, Consistency tests of classical and quantum models for a quantum annealer, Phys. Rev. A **91**, 042314 (2015).

[40] T. Albash, I. Hen, F. M. Spedalieri, and D. A. Lidar, Reexamination of the evidence for entanglement in a quantum annealer, Phys. Rev. A **92**, 062328 (2015).

[41] T. Albash and J. Marshall, Comparing Relaxation Mechanisms in Quantum and Classical Transverse-Field Annealing, Phys. Rev. Appl. **15**, 014029 (2021).

[42] D. Xu and J. Cao, Non-canonical distribution and non-equilibrium transport beyond weak system-bath coupling regime: A polaron transformation approach, Front. Phys. **11**, 110308 (2016).

[43] U. Weiss, *Quantum Dissipative Systems* (World Scientific, Singapore, 2012), 4th ed.

[44] S. Boixo, V. N. Smelyanskiy, A. Shabani, S. V. Isakov, M. Dykman, V. S. Denchev, M. H. Amin, A. Y. Smirnov, M. Mohseni, and H. Neven, Computational multiqubit tunnelling in programmable quantum annealers, Nat. Commun. **7**, 10327 (2016).

[45] S. W. Shin, G. Smith, J. A. Smolin, and U. Vazirani, How "Quantum" is the D-Wave Machine?, (2014), arXiv e-prints, arXiv:1401.7087.

[46] J. A. Smolin and G. Smith, Classical signature of quantum annealing, Front. Phys. **2**, 1 (2014).

[47] D. Subires, F. J. Gómez-Ruiz, A. Ruiz-García, D. Alonso, and A. del Campo, Benchmarking quantum annealing dynamics: The spin-vector Langevin model, Phys. Rev. Res. **4**, 023104 (2022).

[48] J. R. Klauder, Path integrals and stationary-phase approximations, Phys. Rev. D **19**, 2349 (1979).

[49] P. J. D. Crowley and A. G. Green, Anisotropic Landau-Lifshitz-Gilbert models of dissipation in qubits, Phys. Rev. A **94**, 062106 (2016).

[50] V. Choi, Minor-embedding in adiabatic quantum computation: I. The parameter setting problem, Quantum Inf. Process. **7**, 193 (2008).

[51] S. Blanes, F. Casas, J. Oteo, and J. Ros, The magnus expansion and some of its applications, Phys. Rep. **470**, 151 (2009).

[52] G. Lindblad, On the generators of quantum dynamical semigroups, Commun. Math. Phys. **48**, 119 (1976).

[53] R. Kubo, Statistical-mechanical theory of irreversible processes. I. General theory and simple applications to magnetic and conduction problems, J. Phys. Soc. Jpn. **12**, 570 (1957).

[54] P. C. Martin and J. Schwinger, Theory of many-particle systems. I, Phys. Rev. **115**, 1342 (1959).

[55] R. Haag, N. M. Hugenholtz, and M. Winnink, On the equilibrium states in quantum statistical mechanics, Commun. Math. Phys. **5**, 215 (1967).

[56] *D-Wave System Documentation: Annealing implementation and controls* (), available at https://docs.dwavesys.com/docs/latest/c˙qpu˙annealing.html.

[57] *D-Wave System Documentation: Solver Parameters* (), available at https://docs.dwavesys.com/docs/latest/c˙solver˙parameters.html.

[58] F. Yan, S. Gustavsson, A. Kamal, J. Birenbaum, A. P. Sears, D. Hover, T. J. Gudmundsen, D. Rosenberg, G. Samach, S. Weber, J. L. Yoder, T. P. Orlando, J. Clarke, A. J. Kerman, and W. D. Oliver, The flux qubit revisited to enhance coherence and reproducibility, Nat. Commun. **7**, 12964 (2016).

[59] C. M. Quintana, *et al.*, Observation of Classical-Quantum Crossover of $1/f$ Flux Noise and its Paramagnetic Temperature Dependence, Phys. Rev. Lett. **118**, 057702 (2017).